



**HAL**  
open science

# Numerical modeling of non-planar hydraulic fracture propagation in brittle and ductile rocks using XFEM with cohesive zone method

Hanyi Wang

► **To cite this version:**

Hanyi Wang. Numerical modeling of non-planar hydraulic fracture propagation in brittle and ductile rocks using XFEM with cohesive zone method. *Journal of Petroleum Science and Engineering*, 2015, 135, pp.127-140. 10.1016/j.petrol.2015.08.010 . hal-01626428

**HAL Id: hal-01626428**

**<https://hal.science/hal-01626428v1>**

Submitted on 30 Oct 2017

**HAL** is a multi-disciplinary open access archive for the deposit and dissemination of scientific research documents, whether they are published or not. The documents may come from teaching and research institutions in France or abroad, or from public or private research centers.

L'archive ouverte pluridisciplinaire **HAL**, est destinée au dépôt et à la diffusion de documents scientifiques de niveau recherche, publiés ou non, émanant des établissements d'enseignement et de recherche français ou étrangers, des laboratoires publics ou privés.

# Numerical Modeling of Non-Planar Hydraulic Fracture Propagation in Porous Medium using XFEM with Cohesive Zone Method\*

HanYi Wang, University of Texas at Austin

## Abstract

With the increasing wide use of hydraulic fractures in the petroleum industry it is essential to accurately predict the behavior of fractures based on the understanding of fundamental mechanisms governing the process. For unconventional resources exploration and development, hydraulic fracture pattern, geometry and associated dimensions are critical in determining well stimulation efficiency. Multi-stranded non-planar hydraulic fractures are often observed in shale gas stimulation sites. Non-planar fractures propagating from wellbores inclined from the direction of maximum horizontal stress have also been reported. Current computational methods for the simulation of hydraulic fractures generally assume single, symmetric and planar crack geometries, which severely limits the applicability of these methods in predicting complex fracture geometry. In addition, the prevailing approach for hydraulic fracture modeling also relies on Linear Elastic Fracture Mechanics (LEFM), which uses stress intensity factor at the fracture tip as fracture propagation criteria. Even though LEFM can predict hard rock hydraulic fracturing processes reasonably, but often fails to give accurate predictions of fracture geometry and propagation pressure in ductile/unconsolidated formations, even in the form of simple planar geometry. In this study, we present a fully coupled non-planar hydraulic fracture propagation model in permeable medium based on the Extended Finite Element Method (XFEM), and the arbitrary solution-dependent fracture path can be determined by solving a set of discontinuity equations. The Cohesive Zone Method (CZM), which is able to model crack initiation and growth by considering process zone effects, is implemented at the crack tip to enable the modeling of fracture propagation in both brittle and ductile formations. To illustrate the capabilities of the model, example simulations are presented including ones involving non-planar hydraulic fracture growth that initiated from an unfavorable perforation direction. The results indicate that the model is able to capture the development of non-planar hydraulic fracturing propagation in both brittle and ductile formations. The method represents a useful step towards the prediction of non-planar, complex hydraulic fractures and can provide us a better guidance of design wells and hydraulic fractures that will better drain reservoir volume in formation with complex stress conditions and heterogeneous properties.

**Keywords:** hydraulic fracturing; XFEM; cohesive zone method; Non-planar; complex fracture; brittle; ductile

## Introduction

Hydraulic fracturing has been widely used as a common practice to enhance the recovery of hydrocarbons from low permeability reservoirs and prevent sand production in high permeability reservoirs (Economides and Nolte, 2000). Recently, a significant increase in shale gas production has resulted from hydraulic fracturing, which is used to create extensive artificial fractures around (generally cased and cemented) wellbores. When combined with horizontal drilling, the hydraulic fracturing may allow formerly unpractical shale layers to be commercially viable. And understanding fracture initiation and propagation from wellbores is essential for performing efficient hydraulic fracture stimulation treatment.

As a stimulation tool, the problem of hydraulic fracturing is in essence one of predicting the shape of the fracture as a function of time, given the fluid pressure at the wellbore or the flow rate into the fracture. Even today, modeling fluid-driven fracture propagation is still a challenging problem. The mathematical formulation of the problem is represented by a set of nonlinear integro-differential equations. Also, the problem has a moving boundary where the governing equations degenerate and become singular. The complexity of the problem often restricts researchers to consider only simple fracture geometries, such as the KGD model (Khristianovich and Zheltov, 1955; Geertsma and de Klerk, 1969) and PKN model (Perkins and Kern, 1961; Nordgren, 1972). However, under certain circumstances, the hydraulic fracture may evolve in a complex non-planar fashion due to various reasons, such as heterogeneous formation properties, intersection with natural fractures, initiated at an unfavorable orientation and stress interference with by other hydraulic fractures. This in turn can significantly alter the relationship between the injection history and the crack geometry that predicted by planar fracture models, so it is crucial to model non-planar hydraulic fracture propagation in order to understand its impact on the completion process and/or to ensure that undesirable situations do not arise.

In recent years, the extended finite element method (XFEM) has emerged as a powerful numerical procedure for the analysis of fracture problems. This method greatly facilitates the discretization of complex fractures since the finite element mesh is not required to fit crack surfaces. The displacement discontinuity across the crack surfaces approximated through discontinuous enrichment functions. Likewise, the singularity of the linear elastic solution along the crack front is approximated by properly selected enrichment functions (Karihaloo and Xiao, 2003). Since the introduction of this method, the XFEM has been used to model complex, non-planar hydraulic fracture propagations by many authors (Lecampion, 2009; Dahi-Taleghani and Olson, 2011; Meschke and Leonhart, 2011; Gordeliy and Peirce, 2013).

However, an assumption commonly made in all these proposed XFEM models are that the loss of fluid into the rock is evaluated using a one-dimensional diffusion equation and the mechanics of fracture opening and fluid loss are considered

\*:1) This is uncorrected proof

2) Citation Export: Wang, H. 2015. Numerical modeling of non-planar hydraulic fracture propagation in brittle and ductile rocks using XFEM with cohesive zone method. *Journal of Petroleum Science and Engineering*, 135, 127-140.  
<http://dx.doi.org/10.1016/j.petrol.2015.08.010>

independent and their interaction is not considered, so the pressure diffusion and porous behavior of the rock deformation are not fully coupled. In addition, all these models are under the assumptions of linear elastic fracture mechanics (LEFM), which uses stress intensity factor at the fracture tip as fracture propagation criteria. Although hydraulic fracturing simulators based on LEFM can give reasonable predictions for hard rock formation, they fail to predict fracture net pressure and geometry with enough certainty in soft/ductile formation, even in the case of simple, planar fracture geometry. Numerous study and surveys have indicated that the net pressure observed in the field in soft/ductile formations are much higher than that predicted by LEFM and this disparity is even larger in poorly consolidated formations. These observations have triggered a series of dedicated studies which looked into the importance of the plastic deformation in hydraulic fracturing (Papanastasiou, 1997; Germanovich, 1998; Papanastasiou, 1999; Van Dam, 2002). Laboratory studies have also shown that deformation of very weak non-cemented sands and shales can even occur through elastic-visco-plastic constitutive behavior, and the deformations of these types of rocks cannot be predicted by linear elasticity (Sone and Zoback, 2011).

In order to model hydraulic fracture propagation in soft/ductile formations, cohesive zone method (CZM) has been adopted by many authors to model fracture initiation and propagation. The conception of cohesive zone was first introduced by Barenblatt (1959; 1962) to investigate fracture propagation in perfectly brittle materials. In order to investigate fracture damage behavior in ductile materials with small scale of plasticity, a fracture process zone was proposed by Dugdale (1960), that adopt a critical opening condition as a fracture criterion. The physical meaningless tip singularity predicted by LEFM can be resolved with the idea of cohesive zone, which is a region ahead of the crack tip that is characterized by micro-cracking along the crack path, and the main fracture is formed by interconnection of these micro cracks due to damage evolution. Based on this conception, Mokryakov (2011) proposed an analytical solution for hydraulic fracture with Barenblatt's cohesive tip zone, it demonstrates that the derived solutions from cohesive tip zone model can fit the pressure log much more accurately than LEFM for the case of fracturing soft rock. Yao (2012) developed a 3D cohesive zone model to predict fracture propagation in brittle and ductile rocks and the effective fracture toughness method was proposed to consider the fracture process zone effect on the ductile rock fracture. The results show that in ductile formations, the pore pressure cohesive zone model gives predictions that are more conservative on fracture length as compared with pseudo 3D and PKN models. Wang et al. (2014) developed a hydraulic fracture model for both poroelastic and poroplastic formations with the cohesive zone method. Their work indicates that plastic deformation during fracturing execution can lead to higher propagation pressure, shorter and wider fracture geometry. It also found that effects of formation plasticity on fracture propagation are mostly controlled by in-situ stress, plastic property and pore pressure, and the effects plastic deformation in the bulk formation cannot be fully represented by imposing an artificial increased toughness at the fracture tip. However, all these CZM models proposed in literature require a pre-define path for fracture propagation, which severely limits the applicability of these methods in predicting complex fracture geometry.

In this study, a fully coupled, non-planar hydraulic fracture model was developed and for the first time, XFEM combined with CZM was introduced together to model hydraulic fracture propagation in brittle and ductile formations. The physical process involves fully coupling of the fluid leak-off from fracture surface and diffusion into the porous media, the rock deformation and the fracture propagation. XFEM is implemented to determined solution dependent fracture path and CZM is used to model fracture initiation and damage evolution. Example simulations are presented involving non-planar fracture growth and propagation that initiated from a non-favorable perforation angle to illustrate the capabilities of the model.

## **Mathematical Framework**

Following fracture initiation, further fluid injection results in fracture propagation. the geometry of the created fracture can be approximated by taking into account the mechanical properties of the rock, the properties of the fracturing fluid, the conditions with which the fluid is injected (rate, pressure), and the stresses and stress distribution in the porous medium. In describing fracture propagation, which is a particularly complex phenomenon, two sets of laws are required: (i) Fundamental principles such as the laws of conservation of momentum, mass and energy, and (ii) criteria for propagation that include interactions of rock, fluid and energy distribution.

### **Fluid Flow**

A wide variety of fluids have been used for fracturing including water, aqueous solutions of polymers with or without crosslinkers, gelled oils, viscoelastic surfactant solutions, foams, and emulsions. Most hydraulic fracturing fluids exhibit power law rheological behavior and temperature-related properties. In order to avoid additional complexity added by fluid behavior, incompressible and Newtonian fluid is assumed in this study. **Fig. 1** shows a sketch of fluid-driven hydraulic fracture with vary aperture.

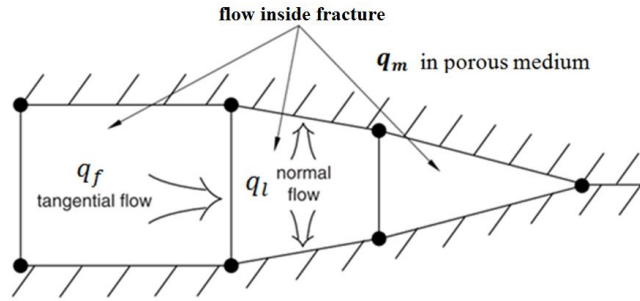


Fig. 1–Sketch of a plane-strain hydraulic fracture with varying aperture

For a flow between parallel plates, local tangential flow rate  $q_f$  can be determined by the pressure gradient to the fracture width for a Newtonian fluid of viscosity  $\mu$  (Boone and Ingraffea, 1990):

$$q_f = -\frac{w^3}{12\mu} \nabla p_f, \dots \dots \dots (1)$$

where  $w$  is the crack aperture,  $p_f$  is the fluid pressure inside the fracture and  $\mu$  is the average fluid viscosity over the cross-section of fracture. Pressure drop along the fracture can be determined by Eq. 1 with local flow rate and local fracture width. The conservation of the fluid mass inside the fracture can be described by the Reynolds (lubrication) equation:

$$\nabla q_f - \frac{\partial w}{\partial t} + q_l = 0, \dots \dots \dots (2)$$

where  $q_l$  is the local fluid loss in rock formation per unit fracture surface area. The local flow rate  $q_f$  can be determined by taking fluid leak-off into consideration. Pressure dependent leak-off model is used in this study to describe the normal flow from fracture into surrounding formations:

$$q_l = c_l(p_f - p_m), \dots \dots \dots (3)$$

where  $p_m$  is pore pressure in the formation and  $c_l$  is fluid leak-off coefficient, which can be interpreted as the permeability of a finite layer of material on the cracked surfaces. Darcy's Law is used to describe fluid diffusion in the porous media:

$$q_m = -\frac{k}{\mu} \nabla p_m, \dots \dots \dots (4)$$

where  $q_m$  is the fluid flux velocity vector in the porous media,  $k$  is formation permeability tensor.

### Coupled Deformation-Diffusion Phenomena

The basic theory of poroelasticity in which the fully coupled linear elastic rock deformation and pore pressure equations was initially introduced by the pioneering work of Biot (1941). Since then, many researchers have contributed to its further development. In fluid filled porous media, the total stresses  $\sigma_{i,j}$  are related to the effective stresses  $\sigma'_{i,j}$  through:

$$\sigma_{i,j} = \sigma'_{i,j} + \alpha p_m, \dots \dots \dots (5)$$

The effective stresses govern the deformation and failure of the rock, the poroelastic constant  $\alpha$  is a rock property that is independent of the fluid properties. Ghassemi (1996) demonstrated that variations in the value of poroelastic constant  $\alpha$  has no influence on fracture geometry. In this study, the poroelastic constant  $\alpha$  is assumed to be 1 and the equilibrium equation in the form of virtual work principle for the volume under its current configuration at time  $t$  can be written as (Zienkiewicz and Taylor 2005):

$$\int_V (\sigma' + p_m \mathbf{I}) : \delta \varepsilon dV = \int_S \mathbf{t} \delta v dS + \int_V \mathbf{f} \delta v dV, \dots \dots \dots (6)$$

where  $\sigma'$ ,  $\delta \varepsilon$  are effective stress and virtual rate of deformation respectively.  $\mathbf{t}$  and  $\mathbf{f}$  are the surface traction per unit area and body force per unit volume,  $\mathbf{I}$  is unit matrix. This equation is discretized using a Lagrangian formulation with displacements as the nodal variables. The porous medium is thus modeled by attaching the finite element mesh to the solid phase that allows

liquid to flow through. A continuity equation required for the fluid, equating the rate of increase in fluid volume stored at a point to the rate of volume of fluid flowing into the point within the time increment:

$$\frac{d}{dt} \left( \int_V \rho_f \phi dV \right) + \int_S \rho_f \phi \mathbf{n} \cdot \mathbf{q}_m dS = 0, \dots \dots \dots (7)$$

where  $\rho_f$  and  $\phi$  are the density of the fluid and porosity of the porous media respectively.  $\mathbf{n}$  is the outward normal to the surface S. The continuity equation is integrated in time using the backward Euler approximation and discretized with finite elements using pore pressure as the variable.

**XFEM Approximation**

The extended finite element method was first introduced by Belytschko and Black (1999). It is an extension of the conventional finite element method based on the concept of partition of unity by Melenk and Babuska (1996), which allows local enrichment functions to be easily incorporated into a finite element approximation. The presence of discontinuities is ensured by the special enriched functions in conjunction with additional degrees of freedom. Thereby, it enables the accurate approximation of fields that involve jumps, kinks, singularities, and other non-smooth features within elements.

For the purpose of fracture analysis, the enrichment functions typically consist of the near-tip asymptotic functions that capture the singularity around the crack tip and a discontinuous function that represents the jump in displacement across the crack surfaces. The approximation for a displacement vector function  $\mathbf{u}$  with the partition of unity enrichment is (Fries and Baydoun, 2012):

$$\mathbf{u} = \sum_{I=1}^N N_I(x) [\mathbf{u}_I + H(x) \mathbf{a}_I + \sum_{\alpha=1}^4 F_{\alpha}(x) \mathbf{b}_I^{\alpha}], \dots \dots \dots (8)$$

where  $N_I(x)$  are the usual nodal shape functions; the first term on the right-hand side of the above equation,  $\mathbf{u}_I$ , is the usual nodal displacement vector associated with the continuous part of the finite element solution; the second term is the product of the nodal enriched degree of freedom vector,  $\mathbf{a}_I$ , and the associated discontinuous jump function  $H(x)$  across the crack surfaces; and the third term is the product of the nodal enriched degree of freedom vector,  $\mathbf{b}_I^{\alpha}$ , and the associated elastic asymptotic crack-tip functions,  $F_{\alpha}(x)$ . The first term on the right-hand side is applicable to all the nodes in the model; the second term is valid for nodes whose shape function support is cut by the crack interior; and the third term is used only for nodes whose shape function support is cut by the crack tip. **Fig. 2** illustrates the discontinuous jump function across the crack surfaces

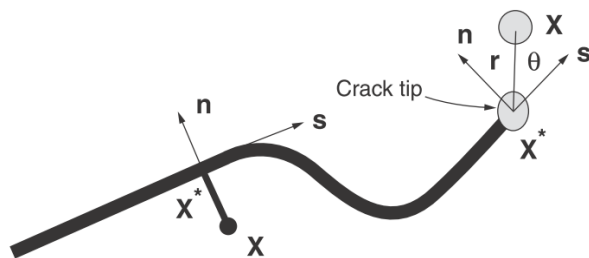


**Fig. 2—Illustration of normal and tangential coordinates for a smooth crack**

And the discontinuous jump function has the following form:

$$H(x) = \begin{cases} 1 & \text{if } (x - x^*) \cdot \mathbf{n} \geq 0 \\ -1 & \text{otherwise} \end{cases}, \dots \dots \dots (9)$$

where  $x$  is a sample (Gauss) point,  $x^*$  is the point on the crack closest to  $x$ , and  $\mathbf{n}$  is the unit outward normal to the crack at  $x^*$ . In Fig.2,  $r$  and  $\theta$  denote local polar coordinates system with its origin at the crack tip and  $\theta = 0$  is tangent to the crack at the tip. The asymptotic crack tip function,  $F_{\alpha}(x)$ , can be determined by (Lecampion, 2009):

$$F_{\alpha}(x) = [\sqrt{r} \sin \frac{\theta}{2}, \sqrt{r} \cos \frac{\theta}{2}, \sqrt{r} \sin \theta \sin \frac{\theta}{2}, \sqrt{r} \sin \theta \cos \frac{\theta}{2}], \dots \dots \dots (10)$$

The above functions can reproduce the asymptotic mode I and mode II displacement fields in LEFM, which represent the near-tip singular behavior in strains and stresses. The use of asymptotic crack-tip functions is not restricted to crack modeling in an isotropic elastic material. The same approach can be used to represent a crack along a bimaterial interface, impinged on the bimaterial interface, or in an elastic-plastic power law hardening material. However, in each of these three cases different forms of asymptotic crack-tip functions are required depending on the crack location and the extent of the inelastic material

deformation. The different forms for the asymptotic crack-tip functions are discussed by Sukumar (2004), Sukumar and Prevost (2003), and Elguedj (2006), respectively. However, accurately modeling the crack-tip singularity requires constantly keeping track of where the crack propagates and is cumbersome because the degree of crack singularity depends on the location of the crack in a non-isotropic material. Therefore, moving cracks are modeled with the cohesive zone method and phantom nodes in this study.

A key development that facilitates treatment of cracks in an XFEM analysis is the description of crack geometry, because the mesh is not required to conform to the crack geometry. The level set method (Osher and Fronts, 1988), which is a powerful numerical technique for tracking interfaces and shapes, fits naturally with the XFEM and makes it possible to model arbitrary crack growth without remeshing. To fully characterize a crack, two orthogonal signed distance functions are needed. The first,  $\phi$ , describes the crack surface, while the second,  $\psi$ , is used to construct an orthogonal surface so that the intersection of the two surfaces gives the crack front, as illustrated in **Fig.3**. Crack growth is modelled by appropriately updating the  $\phi$  and  $\psi$  functions at each iteration. In the context of XFEM, no explicit representation of the boundaries or interfaces is needed for the crack geometry because they are entirely described by the nodal data.

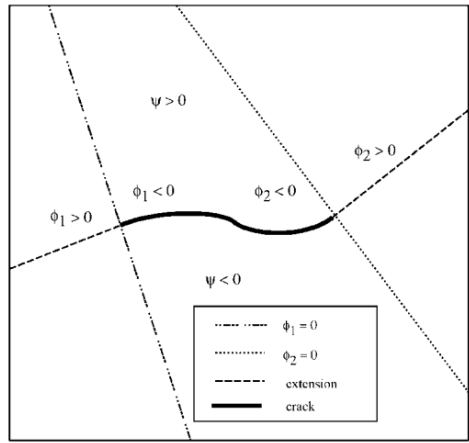


**Fig. 3- Representation of a nonplanar crack by two signed distance functions (Stolarska et al., 2001)**

### Cohesive Zone Method

There is a number of fracture propagation criteria have been proposed by previous studies, which is usually described by either a stress condition or an energy condition. The propagation criterion introduced within the context of LEFM assumes that the process zone, a region near the fracture tip where behavior of the material is not elastic (e.g. region of plastic deformation, microcracking, etc.), is small compared to the fracture size, and a fracture can propagate only if the stress intensity factor exceeds the material toughness. However, fracture propagation in soft/ductile formations can induce a significant plastic deformation around the fracture due to shear failure, which put the adequacy of such assumption into questioning. The cohesive zone model that takes the process zone into consideration is able to capture non-linear fracture mechanics behavior based on energy condition, and a fracture will propagate when the energy release rate in the process zone reaches the critical fracture energy (Barenblatt 1959, 1962).

The constitutive behavior of the cohesive zone is defined by the traction-separation relation, which include initial loading, initiation of damage, and the propagation of damage leading to eventual failure at the bonded surface. The behavior of the interface prior to initiation of damage is often described as linear elastic in terms of a penalty stiffness that degrades under tensile and/or shear loading but is unaffected by pure compression. Laboratory experiments can be used to derive these relations by investigating post-peak behavior with principle/shear stress and axial/shear strain data.

In this study, bilinear cohesive law proposed by Tomar et al. (2004) is used in our model, as shown in **Fig.4**. where  $t_n, t_s, t_t$  refer to the normal, the first, and the second shear stress components; and  $t_n^0, t_s^0, t_t^0$  represent the tensile strength of the rock material when the deformation is purely perpendicular to the interface and the shear strength of rock material in the first and the second shear direction;  $\delta_n^0, \delta_s^0, \delta_t^0$  correspond to the displacement of initial damage in the normal, the first, and the second shear stress direction and  $\delta_n^f, \delta_s^f, \delta_t^f$  are the displacement of complete failure in these three directions. It assumes that the material exhibit linear elastic behavior before the traction reaches the tensile strength / shear strength or the separation of cohesive surfaces exceeds the displacement of damage initiation. Beyond that, the traction reduces linearly to zero up to the displacement of complete failure, and any unloading takes place irreversibly.

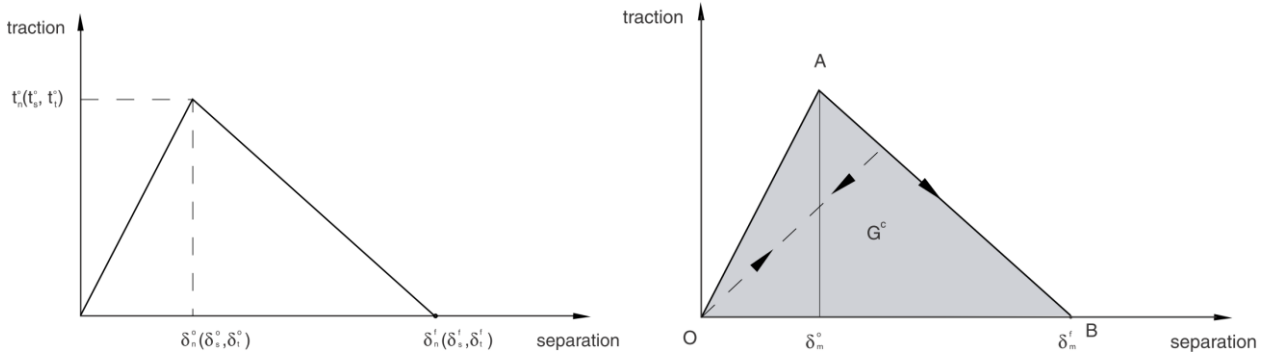


Fig. 4–Linear Traction-Separation law for different modes

Based on loading type, there are three basic crack propagation modes in fracture process. They are named as Mode I (tension, opening), Mode II (shear, sliding), Mode III (shear, tearing), respectively (Simpson et al., 2014). In generally, a crack can generate according to any of these modes or combination of them. For mode-I plane strain fracture, the critical fracture energy  $G_f^c$  equals the area under the traction-separation curve, which can be related to the rock fracture toughness  $K_{IC}$  by (Kanninen and Popelar 1985):

$$G_f^c = \frac{K_{IC}^2}{E} (1 - \nu^2), \dots \dots \dots (11)$$

where  $E$  is Young's modulus of formation and  $\nu$  is Poisson's ratio. Typically, conventional hydraulic fracture models based on LEFM employ Mode-I based fracture criteria that only consider tensile failure mechanism in fracture propagation. However, shear failure can play an important role in soft/ductile formations under certain loading conditions. In this study, the combined effects of different modes will be used to define the damage initial and the propagation criteria in the following discussions.

Damage is assumed to initiate when one of the stress components reaches the value of maximum strength of rock material in that direction, which can be represented by a quadratic law

$$\left\{ \frac{\langle t_n \rangle}{t_n^0} \right\}^2 + \left\{ \frac{t_s}{t_s^0} \right\}^2 + \left\{ \frac{t_t}{t_t^0} \right\}^2 = 1. \dots \dots \dots (12)$$

The symbol  $\langle \ \rangle$  used in the above equation represents the Macaulay bracket with the usual interpretation. The Macaulay brackets are used to signify that a pure compressive deformation or stress state does not initiate damage. The stress components of the traction-separation model are affected by the damage according to

$$\mathbf{t} = \begin{cases} (1 - D)\bar{\mathbf{t}} & \text{damage initiated} \\ \bar{\mathbf{t}} & \text{no damage occurs} \end{cases} \dots \dots \dots (13)$$

where  $\mathbf{t}$  are stress components,  $\bar{\mathbf{t}}$  are the stress components predicted by the elastic traction-separation behavior for the current strains without damage.  $D$  is a scalar damage variable, which has an initial value of 0 and monotonically increases to 1 as damage developing, represents the overall damage that comes from the combined effects of different traction-separation modes in the rock material. For linear softening as shown in Fig. 4, the evolution of the damage variable,  $D$ , reduces to (Turon et al. 2006)

$$D = \frac{\delta_m^f (\delta_m^{max} - \delta_m^0)}{\delta_m^{max} (\delta_m^f - \delta_m^0)}, \dots \dots \dots (14)$$

where  $\delta_m$  is effective displacement, defined as

$$\delta_m = \sqrt{\langle \delta_n \rangle^2 + \delta_s^2 + \delta_t^2}. \dots \dots \dots (15)$$

The mode mix of the deformation fields in the cohesive zone quantify the relative proportions of normal and shear deformation. The the Benzeggagh–Kenane fracture criterion (Benzeggagh and Kenane 1996) is implemented in this model to determine the mixed-mode damage evolution during fracture propagation. This criterion is suitable for situation when the critical fracture energy of rock material along the first and the second shear directions are similar. The combined energy dissipated due to failure  $G^c$ , is defined as

$$G^c = G_I^c + (G_{II}^c - G_I^c) \left( \frac{G_{shear}}{G_{total}} \right)^\eta, \dots \dots \dots (16)$$

where  $G_{shear} = G_{II}^c + G_{III}^c$ ,  $G_{total} = G_{shear} + G_I^c$ . And  $G_I^c, G_{II}^c, G_{III}^c$  are the work done by the tractions and their conjugate relative displacements in the normal, first, and second shear directions. For an isotropic formation, the traction-separation responses in different modes are assumed to be the same in this study, where  $G_{II}^c = G_I^c$ , so the cohesive response is insensitive to parameter  $\eta$ . The fracture will propagate when the energy release rate reaches the value of  $G^c$ . And the newly introduced crack is always orthogonal to the maximum local tensile stress direction when the fracture criterion is satisfied.

Unlike these methods in previous studies (Mokryakov, 2011, Yao, 2012, Wang, 2014), which require that the cohesive zone surfaces align with element boundaries and the cracks propagate along a set of predefined paths, the XFEM-based cohesive zone method can be used to simulate crack initiation and propagation along an arbitrary, solution-dependent path in brittle and ductile materials, since the crack propagation is not tied to the element boundaries in a mesh. In this case the near-tip asymptotic singularity is not needed, and only the displacement jump across a cracked element is considered. Therefore, the crack has to propagate across an entire element at a time to avoid the need to model the stress singularity.

Phantom nodes, which are superposed on the original real nodes, are introduced to represent the discontinuity of the cracked elements (Van de Meer and Sluys, 2009), as illustrated in Fig. 5. When the element is intact, each phantom node is completely constrained to its corresponding real node. When the element is cut through by a crack, the cracked element splits into two parts. Each part is formed by a combination of some real and phantom nodes depending on the orientation of the crack. Each phantom node and its corresponding real node are no longer tied together and can move apart.

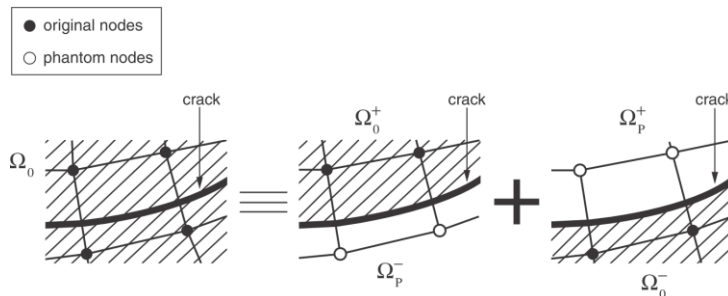


Fig. 4– The principle of the phantom node method (Dassault Systèmes, 2014)

The magnitude of the separation is governed by the cohesive law until the cohesive strength of the cracked element is zero, after which the phantom and the real nodes move independently. To have a set of full interpolation bases, the part of the cracked element that belongs in the real domain,  $\Omega_0$ , is extended to the phantom domain,  $\Omega_p$ . Then the displacement in the real domain can be interpolated by using the degrees of freedom for the nodes in the phantom domain. The jump in the displacement field is realized by simply integrating only over the area from the side of the real nodes up to the crack; i.e.,  $\Omega_0^+$  and  $\Omega_0^-$ . This method provides an effective and attractive engineering approach and has been used for simulation of the initiation and growth of multiple cracks in solids by Song (2006) and Remmers (2008). It has been proven to exhibit almost no mesh dependence if the mesh is sufficiently refined.

### Simulation Model

Because of well stability problems, isolating well from unwanted zones and several other operational considerations, usually wellbores are cased and then perforated; therefore, majority of hydraulic fracturing treatments are performed through perforations. Hydraulic fractures initiate and propagate along a preferred fracture plane (PFP), which is the path of least resistance. In most cases, stress is largest in the vertical direction, so the PFP is vertical and is perpendicular to the minimum horizontal stress. Because perforations control the initial onset of fracture, if the perforations are misaligned with the direction of PFP, the fracture will reorient itself to propagate in the direction of least resistance. This can result in a tortuous path of smaller width, which can result in early screenout from proppant bridging and, eventually, not optimal stimulation treatments. Fig.5 shows the reoriented fractures due to unfavorable perforations.

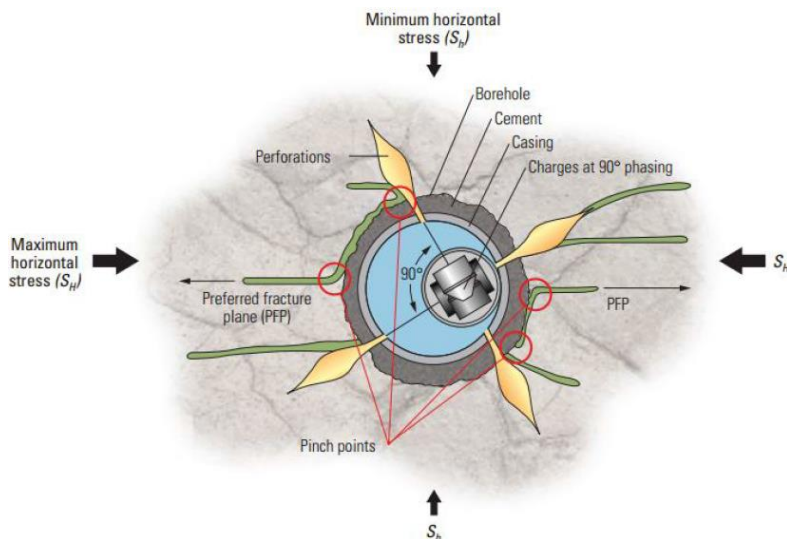
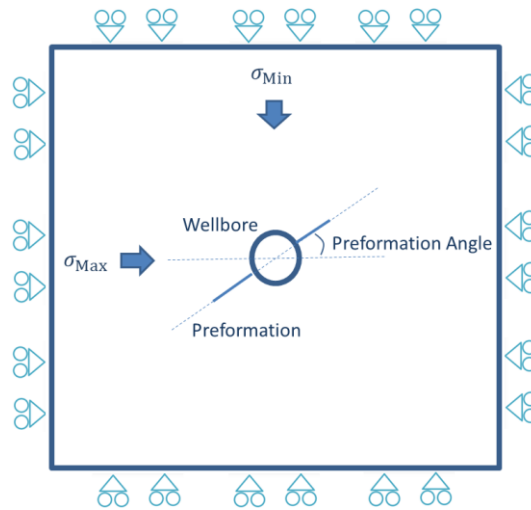


Fig. 5– Reoriented fractures due to unfavorable perforations (Almaguer et al., 2002).



In order to demonstrate our XFEM based CZM model’s capability of capturing non-planar hydraulic fracturing propagation, a near wellbore region with fractures initiated from two different perforation angles are simulated, as shown in **Fig.6**. The fracture path at the perforation points are defined as initially open to allow entry of the fluid at the perforation tunnel(s), so that the initial flow and fracture growth are possible. A dynamic pressure that equals to the fluid pressure at the perforation entry is imposed on the inner surface of wellbore, which will be implicitly calculated by the model during analysis. All the outer boundaries have zero displacement along the direction that perpendicular to its surface, and constant pore pressure condition is imposed on the outer boundaries. The whole simulated regime is saturated with reservoir fluid and incompressible Newtonian fluid is injected at a constant rate at the perforation entries.



**Fig. 6– Graphical representation of wellbore, perforations and stresses**

Besides modeling fracture propagation in brittle formation that undergoes purely elastic deformation, fracture propagation in soft/ductile formation will be also included in this study. The inelastic rock material behavior follows the Mohr-Coulomb flow theory of plasticity for a cohesive frictional dilatant material. Associative behavior with constant dilatation angle is considered here. These assumptions are justified by the presence of high confining stresses prior to crack propagation and to a decrease in the initial in-situ mean pressure near the crack tip during propagation. **Table 1** shows all the input parameters for the simulation.

Input Parameters	Value
Wellbore diameter	0.2 m
Boundary Length	2 m
Perforation Length	0.1 m
Perforation Angle	60°
Elastic modulus	20 GPa
Poisson's ratio	0.25
Fluid viscosity	1 cp
Tensile strength	2 MPa
Formation permeability	50 md
Flow rate	0.00005 (m <sup>3</sup> /s/m)
Specific weight of fluid	9.8 kN/m <sup>3</sup>
Initial pore pressure	10 MPa
Maximum horizontal stress	23 MPa
Minimum horizontal stress	20 MPa
Vertical stress	30 MPa
Critical Fracture Energy	100 J/m <sup>2</sup>
Leak-off coefficient	5E-8 m <sup>3</sup> /s/Pa
Porosity	0.2
Friction angle	27°
Dilation angle	8°
Cohesion strength	3 MPa

Table 1– Input parameters for simulation

The solution procedure is schematically illustrated in **Fig. 6**. The coupled system of non-linear equations is solved numerically by Newton-Raphson method. All the variables in the system are updated at the end of each time increment and input as initial values at the start of the next increment. The program for numerical calculations was developed using FORTRAN and finite element package ABAQUS. Because the fracture has to propagate across an entire element at a time during the simulation,

mesh size has to sufficient small enough to minimize this effect. In this study, the mesh size monotonically decreases from the outer boundary (0.05 m) to the wellbore (0.004 m).

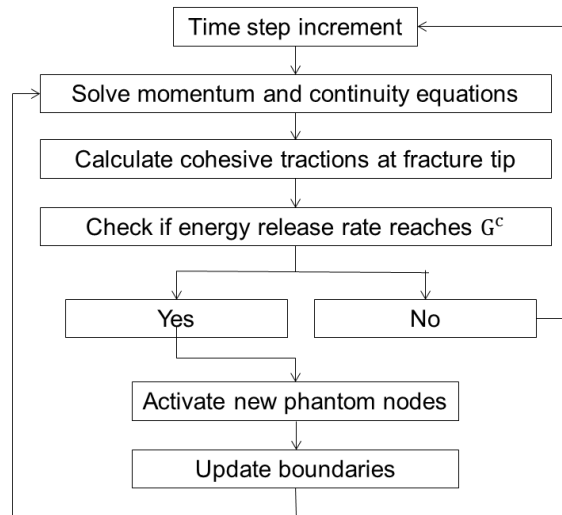


Fig. 6–Solution flow diagram for fracture propagation procedure.

### Results and Analysis

In this section, simulation results are presented to demonstrate the capability of XFEM based CZM to model non-planar hydraulic fracture propagation near the wellbore region, when the direction of perforation is not aligned with the PFP. In addition, fracture propagation in both brittle (elastic rock properties) and ductile (elasto-plastic rock properties) formations are also examined.

Fig. 7 shows the fracture first initiated along the direction of perforation, and then it gradually changes its propagation direction to align itself with the direction of PFP until it hits the simulation boundary. It can be also observed that the shear in-situ stress is intensified in front of fracture tip, where a two wing pattern, shear zone is developed due to local stress disturbance by propagating fracture. It should be mentioned that the displace field presented in all the following results are enlarged by a scale factor of 50, so the fracture geometry and formation deformations can be seen more clearly in the figures.

Fig. 8 shows the formation pore pressure distribution at two different stages. The left figure depicts a moment before hydraulic fracture initiates, when pressure inside the wellbore and perforation channel gradually builds up due to the constant injection of fracturing fluid. Then the fluid begins diffuse into the formation, which leads to higher pore pressure around the wellbore. The right figure depicts a moment when fracture is propagating. It can be observed that a high pressure zone is developed at the fracture tip and a low pressure zone is developed in in front of the fracture tip. The higher pressure zone can be explained by the fact that when a complete new fracture surface is generated within a cell at the fracture tip, there is a sudden fluid leak off into the adjacent formation, due to a large pressure difference between the fluid inside the fracture and the surrounding formation pore fluid. The low pressure zone is developed because of the newly generated fracture volumes by the microcracks (not completely damaged cells) in front of the fracture tip, where it cannot be filled by the fracture fluid.

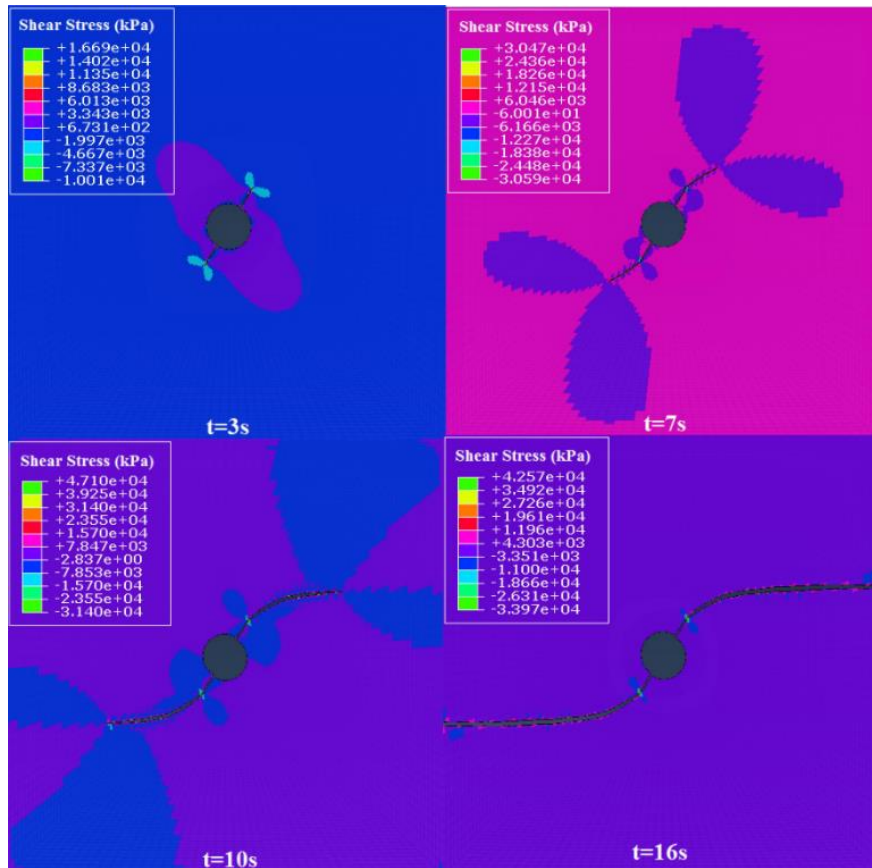


Fig. 7—Shear stress developed during hydraulic fracture propagation.

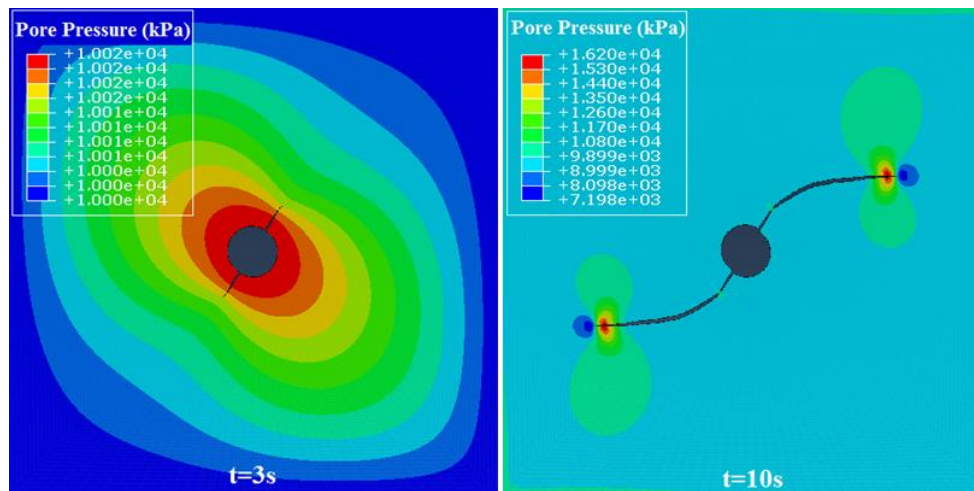


Fig. 8—Pore pressure distribution during hydraulic fracture propagation

**Fig. 9** shows the leak-off rate and cumulative leak-off volume through the surfaces of fractured cells. From the left figure, it can be noticed that the leak-off rate is higher in the newly fractured cells and lower when it is closer to the wellbore (except for those cells that affected by the simulation boundary conditions). This is mainly because the pressure difference between the fluid inside the fracture and the surrounding pores is higher within the newly fractured region. However, as time goes on, leak-off rate will gradually decline because of the increase of surrounding pore pressure due to fluid diffusion. From the right figure, it can be observed that the total cumulative leak-off volume is higher within the fractured cells that closer to the wellbore, this is due to the fact that these cells are fractured earlier, so the exposure time the fracture surface to the fracture fluid is longer and more fracture fluid can leak-off through these surfaces.

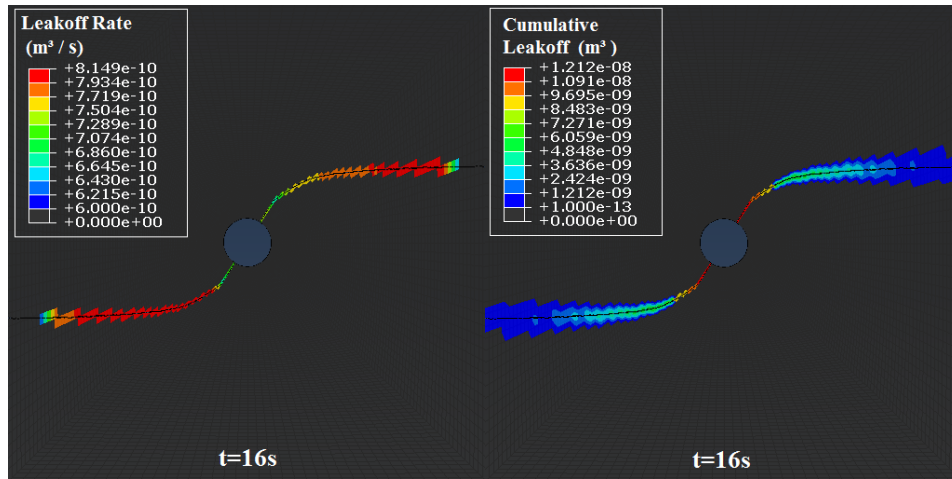


Fig. 9–Leak-off rate and cumulative leak-off volume through fractured cells

Fig. 10 shows the plastic strain and plastic deformation area during hydraulic fracture propagation when formation plasticity is considered in soft/ductile formations. It can be observed that the closer to the fracture surface, the more server the plastic deformation, and plastic deformation area becomes larger when the fracture aligned itself with the direction of PFP. The reason lies behind the plastic deformation is the induced shear stress in front the fracture tip, as depicted by Fig 7.

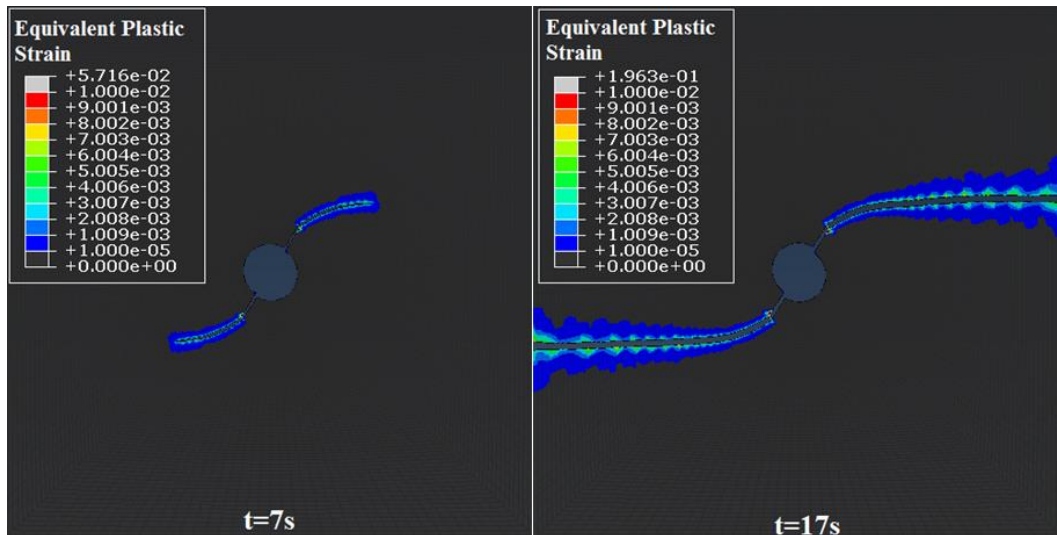


Fig. 10–Plastic strain and plastic deformation during hydraulic fracture propagation

Fig. 11 shows the wellbore pressure and fracture width at the wellbore during hydraulic fracture propagation in both elastic and elasto-plastic formations. It can be observed that the wellbore pressure is almost the same in both formations at initial stage, but pressure in plastic formation gradually surpass the pressure in elastic formation. This is because the plastic deformation region is small initially, so its impact on fracture breakdown pressure is limited, however, as fracture propagates deeper into the formation, more area deformations plastically and in turn, the fracture geometry and wellbore pressure are impacted, this is also the reason for the wider fracture width, that is observed in plastic formation. It can also be noticed that the simulation stops around 16 seconds in the elastic formation, but it runs 1 more second in plastic formation, before the fracture tip hits the simulation boundary. This can be explained by the fact that with wider fracture geometry in the plastic formation, the fracture length is shorter, with the same fluid injection rate in both formations. For more details on how the plastic deformations can impact fracture geometry and fracture propagation pressure beyond the near wellbore region, readers can refer to Wang et al (2014). It should be mentioned that the oscillation of the simulation curves correspond to halts and sequels in the fracture propagation process step by step for the series of time increments. Even though smaller mesh size and simulation time interval can smooth the curves, it can also exert too much burden on computational efforts. So in this paper, the discretization of time and space is a compromise between solution accuracy, numerical convergence and computation time, and the simulation results presented here are still valid to draw general conclusions.

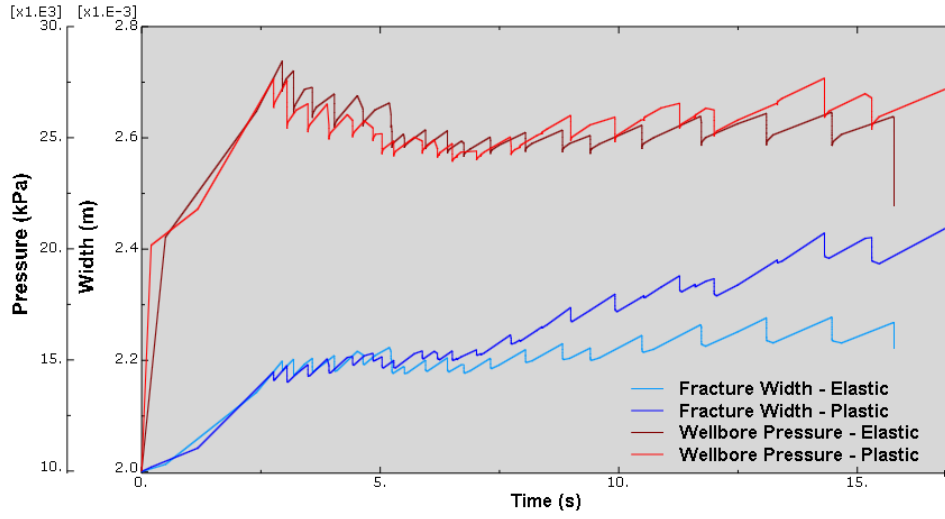


Fig. 11—Fracture width and wellbore pressure for elastic and plastic formations

Even though the model developed in this study can be applied to a broader range of hydraulic fracture applications, such as to investigate fracture initiated from deviated wells, re-fracture process, multiple fractures propagation and interactions under stress shadow, fracture propagation in heterogeneous formations, etc. The investigation of this paper is focusing on the fracture initialization and development in the near wellbore region, to demonstrate the capability of this presented model in capturing the non-planar fracture propagation in both brittle and ductile formations. More applications and case studies of this fully coupled numerical model on hydraulic fracture treatment design and analysis will be investigated in future research efforts.

## Conclusions

In this study, a fully coupled, non-planar hydraulic fracture numerical model was developed and the concept of XFEM combined with CZM was introduced together to model hydraulic fracture process in permeable medium. The physical process involves fully coupling of the fluid leak-off from fracture surface and diffusion into the porous media, the rock deformation and the fracture propagation. XFEM is implemented to determine the arbitrary solution dependent fracture path and CZM is used to model fracture initiation and damage evolution. Example simulations indicated that the presented model is able to capture the initialization and development of non-planar hydraulic fracturing propagation in both brittle and ductile formations. The model developed in this study represents a useful step towards the prediction of non-planar, complex hydraulic fracture evolution and can provide us a better guidance of design wells and hydraulic fractures that will better drain reservoir volume in formations with complex stress conditions and heterogeneous properties.

## Nomenclature

$c_l$	= Leak-off coefficient, $L^2 t/m$ , $m/Pa \cdot s$
$d$	= Initial thickness of cohesive surfaces, $L$ , $m$
$E$	= Young's modulus, $m/Lt^2$ , $Pa$
$f$	= Body force per unit volume, $m/L^2/t^2$ , $N/m^3$
$G$	= Potential function
$G_I^c$	= Fracture critical energy in Mode I, $mL^2/t^2$ , $J$
$G_{II}^c$	= Fracture critical energy in Mode II, $mL^2/t^2$ , $J$
$G_{III}^c$	= Fracture critical energy in Mode III, $mL^2/t^2$ , $J$
$I$	= Unit Matrix
$k$	= Formation permeability tensor in formation, $L^2$ , $md$
$K_n$	= Cohesive stiffness, $m/L^2 t^2$ , $Pa/m$
$p_f$	= Fluid pressure inside fracture, $m/Lt^2$ , $Pa$
$p_m$	= Pore pressure in formation matrix, $m/Lt^2$ , $Pa$
$q_f$	= Flow rate along fracture per unit height, $L^3/t$ , $m^3/s$
$q_l$	= Leakoff rate per unit fracture surface area, $L/t$ , $m^3/(s \cdot m^2)$
$q_m$	= Fluid flux velocity in formation matrix, $L/t$ , $m/s$
$t$	= Surface traction per unit area, $m/L^3 t^2$ , $pa/m^2$
$T$	= Traction force, $m/Lt^2$ , $Pa$
$T_{Max}$	= Cohesive tensile strength, $m/Lt^2$ , $Pa$
$V_L$	= Cumulative leakoff volume, $L^3$ , $m^3$
$w$	= Fracture width, $L$ , $m$
$\alpha$	= Poroelastic constant
$\gamma$	= Shear strain

$\delta$	= Displacement, L, m
$\delta_0$	= Displacement at damage initiation, L, m
$\delta_f$	= Displacement at failure, L, m
$\delta_m$	= Effective displacement, L, m
$\varepsilon$	= Normal strain
$K_{IC}$	= Rock fracture toughness in Mode I, $m/\sqrt{Lt^2}$ , $Pa\sqrt{m}$
$\mu$	= Fluid viscosity, m/Lt, cp
$\nu$	= Poisson's ratio
$v_L$	= Leakoff rate, L/t, m/s
$\rho_f$	= Fluid mass density, $m/L^3$ , $kg/m^3$
$\sigma$	= Stress, $m/Lt^2$ , Pa
$\sigma'$	= Effective stress, $m/Lt^2$ , Pa
$\tau_f$	= Shear strength, $m/Lt^2$ , Pa
$\emptyset$	= Porosity of porous media

## References

- Almaguer, J., Manrique, J., Wickramasuriya, S., López-de-cárdenas, J., May, D., McNally, A. C. and Sulbaran, A. 2002. Oriented Perforating Minimizes Flow Restrictions and Friction Pressures during Fracturing. *Oilfield Review* **14** (1): 16–31. [http://www.slb.com/~media/Files/resources/oilfield\\_review/ors02/spr02/p16\\_31.pdf](http://www.slb.com/~media/Files/resources/oilfield_review/ors02/spr02/p16_31.pdf)
- Barenblatt, G.I. 1959. The formation of equilibrium cracks during brittle fracture: general ideas and hypothesis, axially symmetric cracks. *Journal of Applied Mathematics and Mechanics*, 23:622–636. [http://dx.doi.org/10.1016/0021-8928\(59\)90157-1](http://dx.doi.org/10.1016/0021-8928(59)90157-1).
- Barenblatt, G.I. 1962. The mathematical theory of equilibrium cracks in brittle fracture. *Advanced in Applied Mechanics*. Academic Press, New York, 1962, pp. 55-129.
- Belytschko, T., and T. Black, 1999. Elastic Crack Growth in Finite Elements with Minimal Remeshing. *International Journal for Numerical Methods in Engineering*, vol. 45, pp. 601–620. [http://dx.doi.org/10.1002/\(SICI\)1097-0207\(19990620\)45:5<601::AID-NME598>3.0.CO;2-S](http://dx.doi.org/10.1002/(SICI)1097-0207(19990620)45:5<601::AID-NME598>3.0.CO;2-S)
- Benzeggagh, M.L., and Kenane, M. 1996. Measurement of mixed-mode delamination fracture toughness of unidirectional glass/epoxy composites with mixed-mode bending apparatus. *Composites Science and Technology* 56:439–449. [http://dx.doi.org/10.1016/0266-3538\(96\)00005-X](http://dx.doi.org/10.1016/0266-3538(96)00005-X).
- Biot, M. A. 1941. General theory of three dimensional consolidation. *Journal of Applied Physics*, **12**(2), 155–164. <http://dx.doi.org/10.1063/1.1712886>.
- Boone, T.J., and Ingraffea, A.R. 1990. A numerical procedure for simulation of hydraulically driven fracture propagation in poroelastic media. *International Journal for Numerical and Analytical Methods in Geomechanics*,14:27–47. <http://dx.doi.org/10.1002/nag.1610140103>.
- Boone, T.J., Ingraffea, A.R., and Wawrzynek, P.A. Simulation of fracture process in rock with application to hydrofracturing. *International Journal of Rock Mechanics and Mining Sciences & Geomechanics Abstracts*, 23:255–265. [http://dx.doi.org/10.1016/0148-9062\(86\)90971-X](http://dx.doi.org/10.1016/0148-9062(86)90971-X).
- Dahi-Taleghani, A. and Olson, J. E. 2011. Numerical Modeling of Multistranded-Hydraulic-Fracture Propagation : Accounting for the Interaction between Induced and Natural Fractures. *SPE Journal*, 16(03):575-581. <http://dx.doi.org/10.2118/124884-PA>
- Dassault Systèmes, 2014, ABAQUS 6.14 Analysis User's Guide, Volume (2):864
- Dugdale, D.S. 1960. Yielding of steel sheets containing slits. *Journal of the Mechanics and Physics of Solids*, 8:100–104. [http://dx.doi.org/10.1016/0022-5096\(60\)90013-2](http://dx.doi.org/10.1016/0022-5096(60)90013-2).
- Economides, M. and Nolte, K. 2000. *Reservoir Stimulation*, 3rd edition. Chichester, UK: John Wiley & Sons.
- Elguedj, T., A. Gravouil, and A. Combescure, 2006. Appropriate Extended Functions for X-FEM Simulation of Plastic Fracture Mechanics. *Computer Methods in Applied Mechanics and Engineering*, vol. 195, pp. 501–515. <http://dx.doi.org/10.1016/j.cma.2005.02.007>
- Fries, T. P., and Baydoun, M. 2012. Crack propagation with the extended finite element method and a hybrid explicit-implicit crack description. *International Journal for Numerical Methods in Engineering*. **89**(12), 1527-1558. <http://dx.doi.org/10.1002/nme.3299>
- Geertsma, J. and De Klerk, F. 1969. A rapid method of predicting width and extent of hydraulic induced fractures. *Journal of Petroleum Technology*, 246:1571–1581. SPE-2458-PA. <http://dx.doi.org/10.2118/2458-PA>.

- Germanovich, L.N., Astakhov, D. K., Shlyapobersky, J. et al. 1998. Modeling multi-segmented hydraulic fracture in two extreme cases: No leak-off and dominating leak-off. *International Journal of Rock Mechanics and Mining Sciences*, **35**(4-5), 551- 554. [http://dx.doi.org/10.1016/S0148-9062\(98\)00119-3](http://dx.doi.org/10.1016/S0148-9062(98)00119-3).
- Ghassemi, A. 1996. Three Dimensional Poroelastic Hydraulic Fracture Simulation Using the Displacement Discontinuity Method. PhD dissertation, University of Oklahoma, Norman, Oklahoma.
- Gordeliy, E., and Peirce, A. 2013. Implicit level set schemes for modeling hydraulic fractures using the XFEM. *Computer Methods in Applied Mechanics and Engineering*, 266:125–143, 2013. <http://dx.doi.org/10.1016/j.cma.2013.07.016>.
- Kanninen, M.F., and Popelar, C.H. 1985. *Advanced fracture mechanics*, first edition. Oxford, UK: Oxford University Press.
- Karihaloo, B.L. and Xiao, Q. Z. 2003. Modelling of Stationary and Growing Cracks in FE Framework without Remeshing: A State-of-the-Art Review. *Computers and Structures*, **81** (2003): 119–129. [http://dx.doi.org/10.1016/S0045-7949\(02\)00431-5](http://dx.doi.org/10.1016/S0045-7949(02)00431-5)
- Khristianovich, S., and Zheltov, Y. 1955. Formation of vertical fractures by means of highly viscous fluids. *Proc. 4th World Petroleum Congress, Rome, Sec. II*, 579–586.
- Lecampion, B. 2009. An Extended Finite Element Method for Hydraulic Fracture Problems. *Communication in Numerical Methods in Engineering*, **25**(2): 121–133. . <http://dx.doi.org/10.1002/cnm.1111>
- Leonhart, D., and Meschke, D. 2011. Extended finite element method for hydro-mechanical analysis of crack propagation in porous materials. *Proceedings in Applied Mathematics and Mechanics*, **11**(1):161–162. <http://dx.doi.org/10.1002/pamm.201110072>.
- Melenk, J., and I. Babuska. 1996. The Partition of Unity Finite Element Method: Basic Theory and Applications. *Computer Methods in Applied Mechanics and Engineering*, vol. 39, pp. 289–314. [http://dx.doi.org/10.1016/S0045-7825\(96\)01087-0](http://dx.doi.org/10.1016/S0045-7825(96)01087-0)
- Mokryakov, V. 2011. Analytical solution for propagation of hydraulic fracture with Barenblatt's cohesive tip zone. *International Journal of Fracture*, 169:159–168. <http://dx.doi.org/10.1007/s10704-011-9591-0>.
- Nordgren, R. 1972. Propagation of vertical hydraulic fractures. *Journal of Petroleum Technology*, 253:306–314. SPE-3009-PA . <http://dx.doi.org/10.2118/3009-PA>.
- Osher S, Sethian JA. 1988. Fronts propagating with curvature-dependent speed: Algorithms based on hamilton-jacobi formulations. *Journal of Computational Physics*, vol. 79, pp. 12–49. [http://dx.doi.org/10.1016/0021-9991\(88\)90002-2](http://dx.doi.org/10.1016/0021-9991(88)90002-2)
- Papanastasiou, P. 1997. The influence of plasticity in hydraulic fracturing. *International Journal of Fracture*, **84**(1), 61–79. <http://dx.doi.org/10.1023/A:1007336003057>.
- Papanastasiou, P. 1999. The effective fracture toughness in hydraulic fracturing. *International Journal of Fracture*, **96**(2), 127–147. <http://dx.doi.org/10.1023/A:1018676212444>.
- Perkins, T. and Kern, L. 1961. Widths of hydraulic fractures. *Journal of Petroleum Technology, Trans. AIME*, 222:937–949. <http://dx.doi.org/10.2118/89-PA>.
- Remmers, J. J. C., R. de Borst, and A. Needleman. 2008. The Simulation of Dynamic Crack Propagation using the Cohesive Segments Method. *Journal of the Mechanics and Physics of Solids*, vol. 56, pp. 70–92. <http://dx.doi.org/10.1016/j.jmps.2007.08.003>
- Simpson, N., A. Stroisz, A. Bauer, A. Vervoort, and Holt, R. M. 2014. Failure Mechanics Of Anisotropic Shale During Brazilian Tests, paper presented at 48th US Rock Mechanics/Geomechanics Symposium, American Rock Mechanics Association. ARMA-2014-7399
- Sone, H., and Zoback, M.D. 2011. Visco-plastic Properties of Shale Gas Reservoir Rocks. Presented at the 45th U.S. Rock Mechanics / Geomechanics Symposium, June 26 - 29, San Francisco, California. ARMA-11-417
- Song, J. H., P. M. A. Areias, and T. Belytschko. 2006. A Method for Dynamic Crack and Shear Band Propagation with Phantom Nodes. *International Journal for Numerical Methods in Engineering*, vol. 67, pp. 868–893. <http://dx.doi.org/10.1002/nme.1652>
- Stolarska, M., Chopp, D.L., Moës, N., and Belytschko, T. 2001. Modelling crack growth by level sets in the extended finite element method. *Internat. J. Numer. Methods Engrg.*, 51:943-960. <http://dx.doi.org/10.1002/nme.201>
- Sukumar, N., and J.-H. Prevost. 2003. Modeling Quasi-Static Crack Growth with the Extended Finite Element Method Part I: Computer Implementation. *International Journal for Solids and Structures*, vol. 40, pp. 7513–7537. <http://dx.doi.org/10.1016/j.ijsolstr.2003.08.002>
- Sukumar, N., Z. Y. Huang, J.-H. Prevost, and Z. Suo. 2004. Partition of Unity Enrichment for Bimaterial Interface Cracks. *International Journal for Numerical Methods in Engineering*, vol. 59, pp. 1075–1102. <http://dx.doi.org/10.1002/nme.902>
- Tomar, V., Zhai, J., and Zhou, M. 2004. Bounds for element size in a variable stiffness cohesive finite element model. *International Journal for Numerical Methods in Engineering*, **61**(11): 1894-1920. <http://dx.doi.org/10.1002/nme.1138>.

- Turon, A., Camanho, P.P., Costa, J. et al. 2006. A damage model for the simulation of delamination in advanced composites under variable-model loading. *Mechanics of Materials*, **38** (11): 1072–1089. <http://dx.doi.org/10.1016/j.mechmat.2005.10.003>.
- Van Dam, D.B., Papanastasiou, P., and De Pater, C.J. 2002. Impact of rock plasticity on hydraulic fracture propagation and closure. *SPE Production & Facilities*, **17**(3):149–159. SPE-63172-MS. <http://dx.doi.org/10.2118/63172-MS>.
- Van de Meer, F.P., Sluys, L.J., 2009. A phantom node formulation with mixed mode cohesive law for splitting in laminates. *International Journal of Fracture*. **158**(2):107–124. <http://dx.doi.org/10.1007/s10704-009-9344-5>
- Vermeer, P. A., and de Borst, R. 1984. Non-Associated Plasticity for Soils, Concrete and Rock. *Heron* 29(3): 3-64.
- Wang, H., Marongiu-Porcu, M. and Economides, M. J. 2014. Poroelastic versus Poroplastic Modeling of Hydraulic Fracturing. SPE Paper 168600 presented at the SPE Hydraulic Fracturing Technology Conference held in Woodlands, Texas, USA, 4-6 February. <http://dx.doi.org/10.2118/168600-MS>
- Yao, Y. 2012. Linear Elastic and Cohesive Fracture Analysis to Model Hydraulic Fracture in Brittle and Ductile Rocks. *Rock Mechanics and Rock Engineering*, 45:375–387. <http://dx.doi.org/10.1007/s00603-011-0211-0>.
- Zienkiewicz, O.C., and Taylor, R.L. 2005. *The Finite Element Method*, 5<sup>th</sup> edition, London: Elsevier Pte Ltd.